Submitted July 2018, Revised October 2018

Measured and Calculated Spudcan Penetration Profiles for Case Histories in Sand-over-Clay

Muhammad Shazzad Hossain[1], Pan Hu[2], Mark Jason Cassidy[3], David Menzies[4], and Audrey Wingate[5]

[1] Corresponding Author, Senior Research Fellow (BEng, MEng, PhD, MIEAust), Centre for Offshore Foundation Systems (COFS), The University of Western Australia, 35 Stirling Highway, Crawley, WA 6009, Tel: +61 8 6488 7358, Fax: +61 8 6488 1044, Email: muhammad.hossain@uwa.edu.au

[2] Research Associate (BEng, PhD), Centre for Offshore Foundation Systems (COFS), The University of Western Australia, 35 Stirling Highway, Crawley, WA 6009, Tel: +61 8 6488 4780, Fax: +61 8 6488 1044, Email: pan.hu@uwa.edu.au

[3] Professor (FTSE, FIEAust, GAICD) Dean and Professor of Civil Engineering, Melbourne School of Engineering, Doug McDonell Building, The University of Melbourne, Victoria 3010, Australia, Tel: +61 3 8344 6619, Email: mark.cassidy@unimelb.edu.au

[4] Head of MatthewsDaniel Geotechnical Group, MatthewsDaniel, 4544 Post Oak Place, Suite 160, Houston, Texas 77027, Tel: +1 713 622 1633, Email: davidmenzies@matdan.com

[5] Former Senior Project Engineer, Fugro-McClelland Marine Geosciences, Inc., 6100 Hillcroft (77081), P.O. Box 740010, Houston, Texas 77274, Tel: +1 713 369 5600, Email: Audrey.B.Wingate@gmail.com

- **Number of Words: 5076 (text only)**
- **Number of Tables: 03**
- **Number of Figures: 06**

Measured and Calculated Spudcan Penetration Profiles for Case Histories in Sand-over-Clay

ABSTRACT

This paper reports five case histories of jack-up rig installation in layered soil profiles where a dominate feature was a stronger sand layer overlaying a weaker clay layer. In all cases a relatively continuous load-penetration profile was measured during installation of each of the three spudcan foundations. Summary site-investigation data is provided and consisted of mainly torvane, minature vane, unconsolidated undrained triaxial and pocket penetrometer tests for determining undrained shear strength of the clays and blow counts for deriving the relative density of sand. A statistical averaging method recommended in the InSafeJIP guidelines was used to provide the best fit of the undrained shear strength profile in the clay as this then allowed for spudcan load-penetration profiles to be estimated without introduction of user interpretation or bias. Sand properties were taken as provided in the original site-investigation report. Comparisons between load-penetration profiles calculated using the industry-standard ISO guideline, more recently proposed mechanism-based calculation method and three-dimensional large deformation finite element simulations are made with the measured data, leading to valuable insights for practitioners for estimating behaviour of jack-up installations in problematic sand-over-clay soil profiles.

KEYWORDS: bearing capacity; clays; failure; footings/foundations; numerical modelling; offshore engineering; sands

1 INTRODUCTION

1.1 Spudcan Punch-Through in a Layered Soil

Spudcan-supported jack-up rig installation and preloading in stratified seabed deposits which contain a strong layer of sand over a weak clay layer remains problematic within the offshore industry (Osborne and Paisley 2002; Osborne *et al*. 2009; Jack *et al*. 2013). Punching the sand layer into the weaker clay can cause a rapid penetration, potentially buckling the leg and even toppling the jack-up. Layered soils are prevalent in the Sunda Shelf offshore Malaysia, Australia's Bass Strait and North-West Shelf, the Gulf of Thailand, the South China Sea, offshore Bombay High, the Persian Gulf, and even the Gulf of Mexico (InSafeJIP 2011; Menzies and Lopez 2011).

This background has motivated a number of researchers to explore spudcan penetration in two-layer sand-over-clay soils and multilayer soils with interbedded sand layers (Hanna and Meyerhof 1980; Craig and Chua 1990; Teh *et al*. 2008, 2010; Qiu and Henke 2011; Qiu and Grabe 2012; Tho et al. 2012; Hossain *et al*. 2012; Lee *et al*. 2013a, 2013b; Hossain, 2014; Hu *et al*. 2014a, 2016; Ullah *et al*. 2017a, b) and this has led to new mechanism-based design approaches for assessing spudcan penetration resistance (Teh *et al.* 2009; Lee *et al*. 2009, 2013b; Hu *et al*. 2015a, 2017, 2018). Synthesis of centrifuge model test data and large deformation finite element (LDFE) analysis results have underpinned these new approaches with measured data from jack-up installations in the field rarely reported in the public domain. This hinders an immediate evaluation of the performance of these methods in estimating the spudcan penetration resistance in offshore sand-over-clay deposits. As such, the recently finalised version of ISO guidelines 19905-1 (ISO, 2012) still recommends the 'punching shear' (Hanna and Meyerhof 1980) and 'projected area' (Terzaghi and Peck 1948) methods (see review in Cassidy *et al*. 2015). The approach by Teh et al. (2009) was suggested as an alternative method.

The aim of this paper is to present five case histories of jack-up installations in soil profiles with a dominant sand-over-clay strata. Retrospective estimation of the spudcan load-penetration profiles at each site, calculated using the ISO methods, the mechanism-based approach of Hu *et al*. (2015a, 2017, 2018) and computed using three-dimensional large deformation finite element (LDFE) analyses, are then compared and the lessons learnt are discussed. Only the main methods (punching shear and projected area) suggested in ISO, which are commonly used by the industries, were considered.

1.2 Case Histories

Five case histories were collected from different locations in the Gulf of Mexico, as summarised in Table 1. The field data are reported here for the first time. The soils were two- and four-layer deposits (within the depth of interest) consisting of alternating layers of loose to very dense fine silica sand and soft to stiff clay with an undrained shear strength increasing with depth. The documentation of these case histories includes (a) site-specific soil information, (b) accurate spudcan penetration records (excluding the unload-reload steps), and (c) well-documented spudcan geometries and applied loading. The full details of the soil profiles and spudcan geometries are given in Tables 1 and 2.

1.2.1 Soil investigation and undrained shear strength profile

At each site, a single boring was drilled and sampled by driving thin-wall 2.25-inch (57.15 mm) diameter Shelby tubes and pushing 3.0-in tubes. The samples were wireline driven with a slide-type (165 pounds or 74.84 kg) hammer on a winch that can free fall 5 ft (1.52 m). For clay, the offshore and onshore laboratory tests carried out on the cored samples included the use of (a) pocket penetrometer (PP), (b) torvane, (c) remote vane, (d) miniature vane, and (e) unconsolidated undrained triaxial (UU) tests. In this study, the undrained shear strength, s_u,

profiles are adequately represented using a trend line that increases linearly with depth, which can be expressed as

$$s_u = s_{um} + kz \tag{1}$$

where s_{um} is the undrained shear strength at the sand-clay interface and k is the rate of increase in s_u with depth z. The selection of the design undrained shear strength s_u was based on a statistical method (Lacasse *et al*. 2007; InSafeJIP 2011), with the best linear profile obtained as

$$k = \frac{\sum_{i=1}^{n}\left(z_i - \bar{z}\right)\left(s_{u,i} - \bar{s}_u\right)}{\sum_{i=1}^{n}\left(z_i - \bar{z}\right)^2} \tag{2}$$

$$s_{um} = \bar{s}_u - k\bar{z} \tag{3}$$

where

$$\bar{z} = \frac{1}{n}\sum_{i=1}^{n} z_i$$

$$\bar{s}_u = \frac{1}{n}\sum_{i=1}^{n} s_{u,i}$$

i = 1,…., n is the total number of data points; the design strength profiles for all cases are noted in Table 1. The clays have a sensitivity, S_t, between 1.5 and 3.5, which are derived from the remoulded tests on the cored samples.

For the sand layers, the relative densities were calculated based on blow counts from the hammer sample. The blow counts from the offshore wireline thin-wall Shelby tube sampler

were converted to an SPT N_{60} (blows for 300 mm) value by using a ratio of 1:2 (based on local experience). The N_{60} values were used to calculate the relative densities of the fine sandy soils using the methods proposed by Terzaghi and Peck (1967), Skempton (1986) and Kulhawy and Mayne (1990). The equations and derived average relative densities are listed in Table 3, showing consistent estimation.

The friction and dilation angles were then determined using the general strength-dilatancy framework established by Bolton (1986)

$$I_R = I_D\left[10 - \ln\left(p'\right)\right] - 1 \tag{4}$$

$$\varphi' = 31 + 3I_R \tag{5}$$

$$\psi = \frac{\phi' - 31}{0.48} \tag{6}$$

where I_D is the relative density of the sand; I_R is the dilatancy index, p' is the mean effective stress, and ϕ' and ψ are the friction and dilation angles of the sand, respectively. The values are summarised in Table 1.

1.2.2 Details of spudcan foundations

Two different types of spudcan geometry, hexagonal Marathon LeTourneau Design Class 82-SDC (MLT 82-SDC) and dodecagonal Marathon LeTourneau Design Class 116-C (MLT 116-C), were used for the selected case histories. Figure 1 shows schematic diagrams of the spudcans, and the (plan area) equivalent diameter, plan area, volume, lightship-plus-variable load, maximum preload, and maximum bearing pressure (under the maximum preload) applied during preloading and installation are presented in Table 2. The spudcan (plan area) equivalent diameters, *D*, are 12.1 and 13.5 m, and the bearing pressures range from 309.5 to 390.0 kPa.

2 NUMERICAL ANALYSIS

2.1 Analysis Details

Three-dimensional LDFE analyses were undertaken to simulate the continuous penetration of the spudcans into the seabed surface, providing a complete penetration resistance profile. Spudcan foundation shapes matching the real geometry (including cut-outs, see Figure 1) were considered. The analyses were performed using the Coupled Eulerian-Lagrangian (CEL) approach in the commercial FE package Abaqus/Explicit. The spudcan and soils were discretised using Lagrangian and Eulerian meshes, respectively. The Eulerian mesh was composed of eight-node linear hexahedral elements with reduced integration and hourglass control, while the Lagrangian mesh was composed of four-node linear tetrahedral elements. The Lagrangian elements that move through the Eulerian mesh and the penetration resistance are obtained through contact between the footing and soil materials. The Coulomb friction law was used to describe the frictional footing-sand contact, with the coefficient of friction equal to $\alpha\tan\phi_{cv}$, where α is the footing roughness factor and ϕ_{cv} is the constant-volume friction angle of the sand. Consistent with previous studies by Qiu and Grabe (2012) and Hu *et al*. (2015a), a roughness factor of $\alpha = 0.5$ was adopted in the analyses.

The displacement-controlled mode was used to simulate the penetration of the footing into the sand-over-clay soil. The penetration velocity was specified as 0.2 m/s. The minimum element size and soil domain size were selected based on the convergence study reported by Hu *et al*. (2014b) to achieve adequate numerical accuracy and efficiency and avoid boundary effects. To reduce the computational cost, by taking advantage of the axial symmetry of the geometry of the problem, only a quarter of the domain was modelled. The spudcan penetration depth, *d*, is defined relative to the lowest point of the spudcan's largest cross-section.

2.2 Constitutive Models for Sand and Clay

It was reasonably assumed that the spudcan penetration into sand was under drained conditions and that into clay was under undrained conditions. A brief discussion of the adopted constitutive models is given below, and the details can be found in Hu *et al*. (2015a) and Hossain and Randolph (2009).

For the sand, the traditional Mohr-Coulomb model was modified by varying ϕ and ψ with respect to the accumulated plastic shear strain, ξ. The friction angle was assumed to increase linearly from an initial value ϕ_{ini} to a peak value ϕ_p, before reducing linearly to ϕ_{cv} when the critical state was approached. The peak friction angle ϕ_p was calculated based on both the relative density, I_D, and the mean effective stress applied on the soil, p', following Bolton's (1986) framework (Equations 4~6, with ϕ_{cv} taken as 31°). The threshold plastic shear strains corresponding to ϕ_p and ϕ_{cv} are ξ_p = 4% and ξ_{cv} = 10%, respectively. The incremental plastic shear strain during each incremental step was calculated as

$$\Delta\xi = \frac{\sqrt{6\left[\left(\Delta\varepsilon_1 - \Delta\varepsilon_2\right)^2 + \left(\Delta\varepsilon_2 - \Delta\varepsilon_3\right)^2 + \left(\Delta\varepsilon_3 - \Delta\varepsilon_1\right)^2\right]}}{3} \tag{7}$$

where $\Delta\varepsilon_1$, $\Delta\varepsilon_2$ and $\Delta\varepsilon_3$ are the incremental principal plastic strains measured from the start to the end of the current step. The friction and dilation angles at each integration point are updated for the next step according to the magnitude of deviatoric plastic strain.

The clay was modelled as a linear elastic-perfectly plastic material obeying the Tresca yield criterion, but extended based on the proposed model of Einav and Randolph (2005) and Zhou and Randolph (2007), the Tresca soil model was extended, taking the combined effects of the rate dependency and gradual softening into account. According to the average rate of maximum shear strain in the previous increments and the current accumulated absolute plastic

shear strain, the undrained shear strength at individual Gauss points was modified to

$$s_u = \left[1 + \mu \log\left(\frac{\mathrm{Max}\left(\left|\dot{\xi}\right|, \dot{\xi}_{ref}\right)}{\dot{\xi}_{ref}}\right)\right]\left[\delta_{rem} + \left(1 - \delta_{rem}\right) e^{-3\xi/\xi_{95}}\right] s_{ui} \quad (8)$$

where s_{ui} is the undrained shear strength derived from the boring sample. The first bracketed term augments the strength according to the maximum strain rate, $\dot{\xi}$, relative to a reference value, $\dot{\xi}_{ref}$. Consistent with the triaxial tests in Erbrich (2005) and Lunne *et al*. (2006), $\dot{\xi}_{ref}$ was considered as 1%/h. For a circular spudcan foundation, the rate parameter μ was taken as 0.1 (Low *et al*. 2008). The degradation of strength was modelled in the second part of Equation 8 according to an exponential function of the cumulative shear strain, ξ, from the intact condition to a fully remoulded ratio, δ_{rem} (= $1/S_t$). The parameter ξ_{95} is used to control the relative ductility, representing the cumulative shear strain required for 95% remoulding. Following Randolph (2004), Hossain and Randolph (2009) and Hossain *et al*. (2015), a typical value of ξ_{95} = 15 was considered in this analysis. All the analyses simulated undrained conditions, and a Poisson's ratio of ν = 0.49 was adopted. A uniform stiffness ratio of E/s_u = 500 (where E is the Young's modulus) was taken throughout the clay profile.

Considering the symmetry of the problem, only a quarter spudcan and soil were modelled. The radius and height of the soil domain were 3.25D and 5.0D (as obtained from preliminary convergence study; Hu et al. 2015a), respectively, to ensure that the soil extensions are sufficiently large to avoid boundary effect. A very fine soil mesh was necessary to capture the spudcan-soil contact accurately. Based on the mesh convergence study from Hu et al. (2015a), the typical soil element size along the trajectory of the spudcan was adopted as 0.025D.

3 ANALYTICAL APPROACHES

3.1 Methods

In this study, the two main ISO methods, (a) the load spread method (Terzaghi and Peck 1948; ISO, 2012) and (b) the punching shear method (Hanna and Meyerhof 1980; ISO, 2012), and one mechanism-based design approach (Hu *et al*. 2015a, 2017, 2018) were considered. These methods are discussed briefly below with the full details tabulated in Appendix.

3.1.1 ISO methods

In the load spread method recommended in the ISO guidelines, the bearing capacity of a spudcan, Q_v, is calculated by considering a fictitious footing at the interface between the sand and clay layers according to

$$Q_v = Q_{u,b} - 0.25\pi\left(D + 2\frac{t}{n_s}\right)^2 t\gamma'_s \tag{9}$$

where t is the thickness of the sand layer below the spudcan, n_s is the load spread ratio, and γ'_s is the effective unit weight of sand. The recommended values of the load spread factor n_s are 3 to 5 though lower value was suggested based on actual spudcan penetration data (Baglioni *et al*. 1982). $Q_{u,b}$ is the ultimate vertical foundation bearing capacity for the fictitious footing at the interface between the sand and clay layers with no backfill, which can be calculated as

$$Q_{u,b} = s_u N_c 0.25\pi\left(D + 2\frac{t}{n_s}\right)^2 + \gamma'_s\left[0.25\pi\left(D + 2\frac{t}{n_s}\right)^2 H_s + V_b\right] \tag{10}$$

where V_b is the spudcan volume below the base level. The values of the bearing capacity factor N_c tabulated by Houlsby and Martin (2003) and recommended by the ISO (2012) were used.

The second term of Equation 9 is the weight of the sand plug between the spudcan base and the original sand-clay layer interface.

In the ISO punching shear method, the bearing capacity of a spudcan, Q_v, is calculated assuming a cylindrical failure plane in the sand layer between the base of the foundation and the original sand-clay layer interface (i.e., considering a dilation angle $\psi = 0$). The frictional resistance on the vertical surface of the failure plane and the clay bearing capacity at the base were mobilised, and the bearing capacity was expressed as

$$Q_v = Q_{u,b} - 0.25\pi D^2 t\gamma'_s + 0.5\pi D^2 t\left[t\gamma'_s + 2\gamma'_s\left(H_s - t\right)\right]\frac{K_s \tan\phi'}{D} \quad (11)$$

with

$$Q_{u,b} = s_u N_c\left(0.25\pi D^2\right) + \gamma'_s\left(0.25\pi D^2 H_s + V_b\right) \quad (12)$$

where K_s is the punching shear coefficient, which depends on the strength of both the sand layer and clay layer. It is suggested that the value of this coefficient be obtained from a chart improved from Hanna and Meyerhof (1980).

3.1.2 Hu et al. design approach

Hu *et al*. (2015a, 2017, 2018) proposed a 'mechanism-based' design approach based on the soil flow mechanisms observed in model tests and LDFE analyses. The Hu *et al*. approach simplified the spudcan penetration profile as a combination of the peak resistance and post-peak resistance in the sand layer, q_{peak} and $q_{post\text{-}peak}$, and the resistance in the clay layer, q_{clay}. q_{peak} is the sum of the frictional resistance in the sand, the bearing capacity of the underlying clay and the weight of the sand frustum, and it is expressed as

241
$$q_{\text{peak}} = \left(N_{\text{c0}} s_{\text{um}} + q_0 + 0.12\gamma'_{\text{s}} H_{\text{s}}\right)\left(1+\frac{1.76H_{\text{s}}}{D}\tan\psi\right)^{E^*} + \frac{\gamma'_{\text{s}} D}{2\tan\psi(E^*+1)}\left[1-\left(1-\frac{1.76H_{\text{s}}}{D}E^*\tan\psi\right)\left(1+\frac{1.76H_{\text{s}}}{D}\tan\psi\right)^{E^*}\right] \quad (13)$$

242 where N_{c0} is the bearing capacity factor for clay at the base of a circular foundation, which is
243 obtained from Houlsby and Martin (2003); q_0 is the effective overburden pressure; E^* is a
244 parameter to simplify the algebra. The depth of the peak resistance in the sand layer is taken
245 as $0.12H_{\text{s}}$, where H_{s} is the sand layer thickness.

246 For assessing spudcan penetration resistance after the peak failure in the top sand layer and
247 before penetrating into the bottom clay layer, an analytical model was proposed as

248
$$q = \frac{\gamma'_{\text{s}} D}{E} + \left\{\begin{array}{l}\left[\left(14.8\dfrac{d-0.1H_{\text{s}}}{D}+10.6\right)s_{\text{um}} + q_0 + \gamma'_{\text{s}} H_{\text{s}} + \left(\gamma'_{\text{c}}-\gamma'_{\text{s}}\right)\left(d-0.1H_{\text{s}}\right) - \dfrac{\gamma'_{\text{s}} D}{E}\right] \\ \exp\left[\dfrac{E\left(H_{\text{s}}-d\right)}{D}\right]\end{array}\right\} \quad (14)$$

249 where γ'_{c} is the effective unit weight of clay and E is also a parameter to simplify the algebra
250 (Hu et al. 2018).

251 For the resistance in the clay layer, the bearing capacity is expressed as

252
$$q_{\text{clay}} = N_{\text{c}} s_{\text{u0}} + H_{\text{plug}}\gamma'_{\text{c}} = N_{\text{c}} s_{\text{u0}} + 0.9H_{\text{s}}\gamma'_{\text{c}} \quad \left(0.16 \le \frac{H_{\text{s}}}{D} \le 1.00\right) \quad (15)$$

253 where s_{u0} is the clay shear strength at the lowest level of the spudcan's widest cross-sectional
254 area and H_{plug} is the height of the sand plug. The bearing capacity factor N_{c} was summarised
255 from a sand overlying clay centrifuge testing database and LDFE analyses of the full
256 penetration process, incorporating various footing shapes and soil conditions.

257 The jack-up operators need to understand not only at what load punch-through will occur but

also the depth of penetration during a punch-through event for assessing the consequences of a punch-through failure. The punch-through distance is such an indicator, and it is evaluated as the distance from the depth of q_{peak} to the depth where q_{clay} equals q_{peak} in the underlying clay layer (where equilibrium is re-established) although, in the field, the distance may be controlled by hull buoyancy, which essentially limits the movement of the leg and spudcan. It was used as a basic indicator of the severity of a potential punch-through failure. More details of the equations can be found in Hu *et al*. (2015b).

4 RESULTS AND DISCUSSION

4.1 Comparison among Measured Field Data, Estimation and LDFE Results

Figures 2 to 6 plot the reported spudcan penetration data for Sites 1~5 (Tables 1 and 2), estimations obtained using the design methods, and the results from the 3D LDFE analyses. For the ISO (2012) design methods, the estimations from the load spread method with n_s values of 3 and 5 were made and are presented together with those from the punching shear method. The ISO guideline recommends the use of the expression for N_c given in Houlsby and Martin (2003), so it was adopted for the bearing capacity calculations in the underlying clay layer. For the Houlsby and Martin method, the local shear strength s_{u0} and expressions for the N_c factor considering α = 0.4 (as suggested in SNAME, 2008) were used. For Sites 1-5, the undrained shear strength from the statistical method was used in the predictions and LDFE simulations. As there is a large scatter in the soil strength data for Site 5, and only limited data in 3 metres of clay directly under the sand layer, a weighted average method was also used to derive the shear strength and additional estimation and simulation were made based on this relationship. The following overall comments were obtained by comparing the vertical bearing capacity profiles from field measurements, estimations from design methods and LDFE simulations.

(a) The ISO methods provide good predictions for both the load-penetration profile and punch-through distance for Site 4 but an underprediction of the peak bearing capacity in the remainder. The methods give a reasonably good predictions of punch-through distance for Sites 1 and 5. However, the bearing capacity for Site 2 is significantly under-predicted. For Site 3, a severe punch-through failure is estimated, but a safe installation, with the spudcans rested in the sand layer, was observed in the field.

(b) The load-penetration profiles predicted using the Hu *et al*. approach fit the measured profiles for underlying relatively soft clay (i.e., Sites 1, 2, 3 and 5 (weighted average method)) but the approach overestimates the profiles with underlying stiff clay (i.e., Sites 4 and 5 (statistical average method)).

(c) For Sites 1, 2 and 5 (weighted average method), under the final preload, the spudcan punch-through potential is estimated by the Hu *et al*. approach reasonably well. However, under the preload, no punch-through is estimated for Sites 3, 4 and 5 (statistical average method). For the first case, this conclusion is consistent with field observations, while for the last two cases, the reason is the overestimation of both q_{peak} and q_{clay}.

(d) For each field case, the load-penetration profiles calculated using the load spread and punching shear method in the ISO (2012) guideline provide a lower bound estimate of the bearing capacity, while the Hu *et al*. approach provides a higher estimate of the bearing capacity.

(e) The load-penetration profiles calculated using the Hu *et al*. approach are generally consistent with the computed curves from the LDFE analyses, though with some discrepancies.

With respect to the measured, estimated and computed profiles for each site, further detailed

comments are provided below

(a) *Site 1* (Figure 2): The seabed consisted of four-layer sand and clay soils. The sands were in a loose state, with a relative density of 22.7% and 24.4% for the first and second layers, respectively. Olive grey clay with $s_{um}/\gamma' D$ = 0.18 (first clay layer) and 0.19 (second clay layer) and kD/s_{um} = -0.27 (first clay layer) and 0.99 (second clay layer) formed the second and fourth layers (Figure 2a). The measured load-penetration profiles somewhat increased with depth, and the spudcans finally rested at a deep penetration of d = 15~21 m (Figure 2b). A leg run of 10.5 m to 13 m occurred to the port leg and, under the final preload of 35.5 MN, a settlement of 18.5 m to 21 m occurred to the bow leg. The estimated profiles using both the ISO methods and the Hu *et al*. approach show potential of a severe punch-through failure in the second sand layer. However, the estimated profile from the Hu et al. approach match the measured one in the 2nd sand layer. In the 2nd clay layer, the ISO methods significantly underestimate the penetration resistance except the final penetration depths of the starboard and bow legs. The Hu *et al*. approach provides reasonable estimates up to 12.5 m followed by overestimates except the final penetration depth of the port leg. The bearing capacity-depth profile from the LDFE analysis shows a trend similar to that of the estimated profile using the Hu *et al*. approach in all four soil layers.

(b) *Site 2* (Figure 3): The seabed consisted of medium sand overlying soft clay with $s_{um}/\gamma' D$ = 0.20 and kD/s_{um} = 0.99 (Figure 3a). A number of consistent strength data points led to derive a more accurate strength profile for the clay layer. Under the maximum preload of 53.4 MN, all three legs experienced a severe punch-through with the punch-through distance measured as 15.76~18.50 m (Figure 3b). The spudcans finally rested at d = 15.8~18.5 m. Although the potential for punch-through failure is estimated by the ISO methods and the final penetration depths are well estimated, both

331 the peak bearing capacity in the sand layer and the bearing capacity in the clay layer
332 are significantly underestimated. The Hu *et al*. approach estimates the magnitude and
333 depth of the peak bearing capacity in the sand layer reasonable well, with the
334 difference in terms of the peak bearing capacity being 12%. The punch-through
335 distance is estimated as 10.92 m, which is lower than that obtained from the field
336 measurements. The penetration resistance in the clay layer is significantly
337 overestimated. The computed profile from the LDFE simulation shows almost
338 constant bearing capacity in the top sand layer, which is consistent with the field data.
339 However, it follows the estimated profile using the Hu *et al*. approach in the clay
340 layer. This comparison highlights that a significant number of data points led more
341 accurate clay strength profile improves the estimation accuracy of the Hu *et al*.
342 approach.

343 (c) *Site 3* (Figure 4): The seabed consisted of medium sand (I_D = 63.7%) overlying soft
344 clay with $s_{um}/\gamma' D$ = 0.25 and kD/s_{um} = 0.51 (Figure 4a). This is the only case in which
345 three spudcans rested in the sand layer with no punch-through failure. The measured
346 bearing capacity-depth profiles for the bow leg and starboard leg were similar. The
347 profile for the port leg followed the same trend, although with a slightly greater
348 penetration of 1.6 m, which may be due to the movement of the seabed sand around by
349 currents. The final embedment was d = 1~1.6 m, which was near the sand layer
350 surface (Figure 4b). Under a preload of 35.6 MN, the ISO methods estimate severe
351 punch-through failure immediately after the spudcans penetrate into the sand layer,
352 and the spudcan would penetrate rapidly until the final penetration depth of 15.84 m to
353 balance the maximum preload. The Hu *et al*. approach estimates a peak bearing
354 capacity of 46.6 MN, which indicates that the soil bearing resistance (mainly from the
355 sand in this case) is high enough to resist the preload, and no punch-through failure

would occur. The LDFE analysis again confirms this conclusion by simulating similar trends in both the top sand and the underlying clay layer.

(d) *Site 4* (Figure 5): The seabed consisted of very dense sand overlying stiff clay with higher $s_{um}/\gamma' D$ of 0.42 and kD/s_{um} of 2.06 (Figure 5a) compared to those relatively soft clays at Sites 1~3. Only the Bow leg experienced a punch-through failure from 3.5 to 6.92 m. The other two legs penetration were limited to a shallow depth of d = 3.9~6.9 m (Figure 5b). The profiles using the ISO methods provide reasonable estimation of the measured data. The Hu *et al*. approach overestimates the bearing capacity, and no punch-through failure is estimated under the current preload of 56.0 MN. The reason might be that the peak bearing capacity expression in the Hu *et al*. approach was mainly based on a database of relatively soft underlying clay, and the high shear strength of the clay (with a gradient of 5.71 kPa/m) at this site was beyond the range over which it was originally calibrated. Additionally, only two types of laboratory tests (with 14 data points) were used for deriving the shear strength of the soil, and, as discussed previously, the prediction is sensitive to the quality of the shear strength data. The LDFE analysis also estimates a much higher bearing capacity, but no punch-through failure potential is shown.

(e) *Site 5* (Figure 6): The seabed consisted of medium sand over soft clay with $s_{um}/\gamma' D$ = 0.21 and kD/s_{um} = 1.71 (Figure 6a). Under a preload of V_p = 35.6 MN, the final spudcans embedment depth were in the range of d = 7.4~8.6 m (Figure 6b). All three legs experienced a severe punch-through at a depth of 0.5~1.8 m. The ISO methods provide good estimate of the load-penetration profiles for d/D = 0~0.71, including the peak capacities at punch-through in the sand layer and most of the penetration in the clay layer. In addition, the final penetration depths are well estimated. The Hu *et al*. approach with clay strength derived from the statistical average method, however,

significantly overestimates the bearing capacity in both sand and clay layers. The reason might be the scattered clay strength data in this site with the obvious discrepancy between the average shear strength profile and the site investigation data being particularly in the top 7 m (see Figure 6a). There are less data points in the top and middle parts of the boring log compared to the bottom part, so in another comparison more weight was assigned to the data points of the top 7 m. The Hu *et al*. approach using this weighted average strength profile provides improved estimation in the sand layer including the peak capacity at punch-through. This comparison highlights the importance of adequate data, leading to a more accurate soil strength profile. The computed profile from the LDFE simulation using the weighted average shear strength shows somewhat increasing resistance with depth.

4.2 Lessons Learnt

(a) The quality of the data in the interested depth range is necessary for the accurate estimation of the shear strength of the soil and then the estimation of the bearing capacity-depth profile. The predictions are sensitive to the quality of the site investigation data, with few and scattered data possibly worsening the estimations, as shown for Sites 1, 4 and 5.

(b) The load spread method with a load spread ratio of $n_s = 3$ always estimates a higher bearing capacity than that with a load spread ratio of $n_s = 5$, and the estimated profile lies closer to the field measurements. As such, it is recommended that $n_s = 3$ be adopted for predicting spudcan penetration resistance, at least for locations in the Gulf of Mexico. This is consistent with the observation of Hu et al. (2015b) that $1.73 \leq n_s \leq 2.75$ best fits the field data.

(c) To reduce the subjectivity in the selection of the parameters needed for the bearing capacity analysis, more high quality soil information is better. The volume of information and its reliability may be increased by additional in situ testing and soil borings at each spudcan location and advanced laboratory soil tests that identify and reduce the data scattering and the effects of sample disturbances (Menzies and Roper 2008).

(d) Site 2 and Site 3 are located in the same 4.83 × 4.83 km block. Yet, for site 2, all three spudcans experienced a punch-through and penetrated through the top sand layer while for site 3, all three spudcans rested in the top sand layer although relatively the top sand layer is thinner (7 m for site 2 vs 4.9 m for site 3; relative density similar; Table 1) and the underlying clay layer is slightly stronger (s_{um} = 17.87 vs 22.13 kPa; Table 1). This is chiefly because, as learned from site 3, the applied maximum bearing pressure (under the full preload) has been reduced to of 310.4 kPa for site 3 (from 371.9 kPa at site 2). Otherwise, from Figure 4b, an application of a similar bearing pressure of 371.9 kPa (> ~42 MN full preload) would have resulted in a severe punch-through. The reverse could have been true as well, as relying on the experience of site 3 and without site-specific investigation and prediction, it would have been thought that a pressure of 371.9 kPa could also be applied safely at site 2.

A disastrous consequence of this principle is the punch-through event experienced by the Harvey H. Ward jack-up rig at Anding, offshore of the Malaysian peninsula west coast (Maung and Ahmad 2000). Prior to the installation, the load-penetration resistance was predicted using previously obtained borehole data for another jack-up rig (Trident 17) for the same location showing no existence of an interbedded soft layer. Trident 17 was deployed at Anding without any problem for a maximum preload of 37 MN (bearing pressure of 375 kPa) and provided confidence for further

jack-up installations. Unfortunately, the installation of the Harvey H. Ward rig in 1999 under a maximum preload of 39.5 MN (an equivalent pressure of 344 kPa, lower than that of Trident 17) did not proceed as well. The bow leg punched through at 11 m, which caused the hull to tilt and resulted in bending damage to all three legs. Subsequently, additional soil borings were carried out, and a careful analysis of the data identified a soft clay layer at 13.5 to 17 m under a thin stiff layer at 11 to 13.5 m.

5 CONCLUDING REMARKS

Three different methods for estimating the penetration resistance of spudcans in sand overlying clay soils have been compared with high-quality data from field installations. A brief summary was provided about three design methods, comprising the two ISO (2012) methods and the mechanism-based design approach of Hu *et al*. (2015a, 2017, 2018). Five case histories were considered, all from different locations in the Gulf of Mexico, where the soils were relatively homogeneous, predominantly sand on top of normally to lightly over-consolidated clay with the strength increasing essentially linearly with depth. The data for spudcan penetrations from 0 to 1.7 diameters were compared with the estimations from the design methods and with the results from three-dimensional large deformation finite element (LDFE) analyses.

Where more and higher quality site investigation data were available, the estimations using the Hu *et al*. approach were found to be in agreement with the measured bearing capacity-depth profiles. The profiles estimated using the ISO methods provided (i) lower bound estimates of the bearing capacity of the soils and upper bounds of the spudcan penetration depth, and (ii) the good estimation of the measured data where the site investigation data are less and scattered.

6 ACKNOWLEDGEMENTS

The research presented herein was undertaken in collaboration with Fugro-McClelland Marine Geosciences, Inc., Houston, Texas; and with support from the Australian Research Council (ARC) through the Linkage Project LP140100066. This work forms part of the activities of the Centre for Offshore Foundation Systems (COFS), currently supported as a node of the Australian Research Council Centre of Excellence for Geotechnical Science and Engineering and as a Centre of Excellence by the Lloyd's Register Foundation. The Lloyd's Register Foundation supports the advancement of engineering-related education, and funds research and development that enhances safety of life at sea, on land and in the air. This support is gratefully acknowledged.

7 REFERENCES

Baglioni, V. P., Chow, G. S., and Endley, S. N. (1982). "Jack-up foundation stability in stratified soil profiles." *Proc., 14th Offshore Technology Conf*., Houston, OTC 4409.

Bolton, M. D. (1986). "The strength and dilatancy of sands." *Géotechnique*, 36(1), 65-78.

Cassidy, M. J., Li, J. H., Hu, P., Uzielli, M., and Lacasse, S. (2015). "Deterministic and probabilistic advances in the analysis of spudcan behaviour." *Proc. 3rd Int. Sym. on Frontiers of Offshore Geotechnics*. (ISFOG-2015), Oslo, Norway. Vol. 1, pp. 183-214.

Craig, W. H., and Chua, K. (1990). "Deep penetration of spud-can foundation on sand and clay." *Géotechnique*, 40(4), 541-556.

Einav, I., and Randolph, M. F. (2005). "Combining upper bound and strain path methods for evaluating penetration resistance." *Int. J. Numerical Methods in Engineering*, 63(14), 1991-2016.

Erbrich, C. T. (2005). "Australian frontiers – spudcans on the edge." *Proc. 1st Int. Symp. on Frontiers in Offshore Geotechnics*. (ISFOG-2005), Perth, pp. 49-74.

Hanna, A. M., and Meyerhof, G. G. (1980). "Design charts for ultimate bearing capacity of foundations on sand overlying soft clay." *Can. Geotech. J*., 17(2), 300-303.

Hossain, M. S. (2014). "Experimental investigation of spudcan penetration in multi-layer clays with interbedded sand layers." *Géotechnique*, 64(4), 258-277.

Hossain, M. S., and Randolph, M. F. (2009). "Effect of strain rate and strain softening on the penetration resistance of spudcan foundations on clay." *Int. J. Geomechanics*, 9 (3), 122-132.

Hossain, M. S., and Randolph, M. F. (2012). "Spudcan foundations on multi-layered soils with interbedded sand and stiff clay layers." *Int. J. Offshore and Polar Engineering*, 22 (3), 248-255.

Hossain, M. S., Zheng, J., Menzies, D., Lillian, M., and Randolph, M. F. (2014). "Spudcan penetration analysis for case histories in clay." *J. Geotech. Geoenviron. Engng.*, 140 (7), 04014034-1-13.

Houlsby, G. T., and Martin, C. M. (2003). "Undrained bearing capacity factors for conical footings on clay." *Géotechnique*, 53(5), 513-520.

Hu, P., Stanier, S. A., Cassidy, M. J., and Wang, D. (2014a). "Predicting peak resistance of spudcan penetrating sand overlying clay." *J. Geotech. Geoenviron. Engng.*, 140(2), 04013009-1-12.

Hu, P., Wang, D., Cassidy, M. J., and Stanier, S. A. (2014b). "Predicting the resistance profile of spudcan on sand overlying clay." *Can. Geotech. J.*, 51(10), 1151-1164.

Hu, P., Wang, D., Stanier, S. A., and Cassidy, M. J. (2015a). "Assessing the punch-through hazard of a spudcan on sand overlying clay." *Géotechnique*, 65(11), 883–896.

Hu, P., Stanier, S. A., Wang, D., and Cassidy, M. J. (2015b). "A comparison of full profile prediction methods for a spudcan penetrating sand overlying clay." *Geotech. Lett.*, 5 (3), 131-139.

Hu, P., Stanier, S. A., Wang, D., and Cassidy, M. J. (2016). "Effect of footing shape on penetration in sand overlying clay." *Int. J. Phys. Model. Geo.*, 16(3), 119-133.

Hu, P., and Cassidy, M. J. (2017). "Predicting jack-up spudcan installation in sand overlying stiff clay." Ocean. Eng., 146, 246-256.

Hu, P., Cassidy, M. J., and Randolph, M. F. (2018). "Bearing capacity on sand overlying clay: An analytical model for predicting post peak behaviour." Mar. Struct., 59, 94-104.

InSafeJIP (2011). *Improved guidelines for the prediction of geotechnical performance of spudcan foundations during installation and removal of jack-up units*. Joint Industry Funded Project.

ISO (2012). *Petroleum and natural gas industries – Site specific assessment of mobile offshore units – Part 1: Jack-ups*. International Organization for Standardization, ISO 19905-1.

Jack, R. L., Hoyle, M. J. R., Smith, N. P., and Hunt, R. J. (2013). "Jack-up accident statistics – a further update." *Proc., 14th Int. Conf. on the Jack-up Platform Design, Construction and Operation*, London.

Lacasse, M., Nadim, F., Rahim, A., and Guttormsen, T. R. (2007). "Statistical description of characteristic soil properties." *Proc. Offshore Technology Conf.*, Houston, OTC 19117.

518 Lee, K. K., Randolph, M. F., and Cassidy, M. J. (2009). "New simplified conceptual model
519 for spudcan foundations on sand overlying clay soils." *Proc. Offshore Technology*
520 *Conf.*, Houston, OTC 20012.

521 Lee, K. K., Cassidy, M. J., and Randolph, M. F. (2013a). "Bearing capacity on sand overlying
522 clay soils: Experimental and finite element investigation of potential punch-through
523 failure." *Géotechnique*, 63(15), 1271-1284.

524 Lee, K. K., Randolph, M. F., and Cassidy, M. J. (2013b). "Bearing capacity on sand overlying
525 clay soils: A simplified conceptual model." *Géotechnique*, 63(15), 1285-1297.

526 Low, H. E., Randolph, M. F., DeJong, J. T., and Yafrate, N. J. (2008). "Variable rate full-flow
527 penetration tests in intact and remoulded soil." *Proc. 3rd Int. Conf. on Geotechnical and*
528 *Geophysical Site Characterization*, Taylor & Francis Group, Taipei, Taiwan, pp. 1087-
529 1092.

530 Lunne, T., Berre, T., Andersen, K. H., Strandvik, S., and Sjursen, M. (2006). "Effects of
531 sample disturbance and consolidation procedures on measured shear strength of soft
532 marine Norwegian clays." *Can. Geotech. J.*, 43(7), 726-750.

533 Maung, U. M., and Ahmad, C. K. M. (2000). "Swiss cheesing to bring in a jack-up rig at
534 Anding location." *Proc. IADC/SPE Asia Pacific Drilling Technology Conf.*, Kuala
535 Lumpur, Malaysia. Asia Pacific Drilling Technology, Richardson, Tex. Paper
536 IADC/SPE 62755.

537 Menzies, D., and Lopez, C. R. (2011). "Four atypical jack-up rig foundation case histories."
538 *Proc. 13th Int. Conf. The Jack-up Platform: Design, Construction and Operation*,
539 London.

540 Osborne, J. J., Houlsby, G. T., Teh, K. L., Bienen, B., Cassidy, M. J., Randolph, M. F., and
541 Leung, C. F. (2009). "Improved guidelines for the prediction of geotechnical
542 performance of spudcan foundations during installation and removal of jack-up units."
543 *Proc., Offshore Technology Conf.*, Houston, OTC 20291.

544 Osborne, J. J., and Paisley, J. M. (2002). "SE Asia jack-up punch-throughs: The way
545 forward?" *Proc., the Int. Conf. on Offshore Site Investigation and Geotechnics –*
546 *Sustainability and Diversity*. London, UK, pp. 301-306.

Qiu, G., and Henke, S. (2011). “Controlled installation of spudcan foundations on loose sand overlying weak clay.” *Marine Structures*, 24(4), 528-550.

Qiu, G., and Grabe, J. (2012). “Numerical investigation of bearing capacity due to spudcan penetration in sand overlying clay.” *Can. Geotech. J.*, 49(12), 1393–1407.

Randolph, M. F. (2004). “Characterisation of soft sediments for offshore applications. Keynote lecture.” *Proc. 2nd Int. Conf. Site Characterisation*, Porto 1, 209–231.

Skempton, A. K. (1986). “Standard penetration test procedures and the effects in sands of overburden pressure, relative density, particle size, aging, and overconsolidation.” *Géotechnique*, 36(3), 425–447.

SNAME (2008). *Guidelines for site specific assessment of mobile jack-up units*, T&R Bulletin 5-5 and 5-5A, panes OC-7 site assessment of jack-up rigs. Jersey City, NJ, USA: Society of Naval Architects and Marine Engineers.

Teh, K. L., Cassidy, M. J., Leung, C. F., Chow, Y. K., Randolph, M. F., and Quah, M. (2008). “Revealing the bearing capacity mechanisms of a penetrating spudcan through sand overlying clay.” *Géotechnique*, 58(10), 793-804.

Teh, K. L., Leung, C. F., Chow, Y. K., and Handidjaja, P. (2009). “Prediction of punch-through for spudcan penetration in sand overlying clay.” *Proc. Offshore Technology Conf.*, Houston, OTC 20060.

Teh, K. L., Leung, C. F., Chow, Y. K., and Cassidy, M. J. (2010). “Centrifuge model study of spudcan penetration in sand overlying clay.” *Géotechnique*, 60(11), 825-842.

Terzaghi, K., and Peck, R. B. (1948). “Soil Mechanics in engineering practice.” John Wiley and Sons, New York.

Tho, K. K., Leung, C. F., Chow, Y. K., and Swaddiwudhipong, S. (2012). “Eulerian finite element technique for analysis of jack-up spudcan penetration.” *Int. J. Geomech.*, 12(1), 64-73.

Ullah, S. N., Stanier, S., Hu, Y., and White, D. (2017a). “Foundation punch-through in clay with sand: analytical modelling.” *Géotechnique*, 67(8), 672-690.

Ullah, S. N., Stanier, S., Hu, Y., and White, D. (2017b). “Foundation punch-through in clay with sand: centrifuge modelling.” *Géotechnique*, 67(10), 870-889.

576 Zhou, H., and Randolph, M. F. (2007). “Computational techniques and shear band
577 development for cylindrical and spherical penetrometers in strain-softening clay.” *Int. J.*
578 *Geomech*., **7**(4), 287-295.

579

NOTATION

A	spudcan plan area at largest section
d	penetration depth of spudcan base (lowest point of largest section)
D	foundation plan area equivalent diameter
E	Young's modulus
E^*	parameter to simplify the algebra
H_s	sand layer thickness
I_D	relative density of sand
I_R	dilatancy index
k	rate of increase of undrained strength with depth
K_s	punching shear coefficient
n	load spread ratio
N_c	bearing capacity factor
N_{c0}	bearing capacity factor of clay at base level of a circular foundation
p'	mean effective stress
q_0	effective overburden pressure
q_{clay}	penetration resistance in the clay layer
q_{max}	maximum bearing pressure
q_{peak}	peak resistance in the sand layer
Q_{ub}	ultimate vertical bearing capacity of the fictitious footing
Q_v	vertical bearing capacity of a spudcan
S_t	soil sensitivity
s_u	undrained shear strength
s_{ui}	undrained shear strength derived from the boring sample
s_{um}	undrained shear strength at the sand-clay interface
s_{u0}	local undrained shear strength at spudcan base level, d
t	thickness of the sand layer (below spudcan diameter) in the ISO methods
V	total volume of spudcan beneath backfill (buried volume)
V_b	volume of spudcan below maximum bearing area
V_P	final preload

610	z	depth below soil surface
611	α	footing roughness factor
612	δ_{rem}	remoulded ratio (inverse of sensitivity)
613	σ'_{v0}	effective vertical stress
614	ϕ'	effective friction angle
615	ϕ_{cv}	constant-volume friction angle of the sand
616	ϕ_{ini}	initial value of friction angle
617	ϕ_p	peak friction angle
618	ψ	dilation angle of sand
619	ψ_p	peak dilation angle
620	γ'	effective unit weight of soil
621	γ'_c	effective unit weight of clay
622	γ'_s	effective unit weight of sand
623	μ	rate parameter
624	ν	Poisson's ratio
625	ξ	absolute cumulative plastic shear strain
626	$\dot{\xi}$	maximum shear strain rate
627	$\Delta\xi$	incremental plastic shear strain
628	ξ_{95}	softening parameter
629	ξ_{cv}	plastic shear strains corresponding to critical state
630	ξ_p	plastic shear strains corresponding to peak friction angle
631	$\dot{\xi}_{ref}$	reference shear strain rate at which s_u was assessed
632	$\Delta\varepsilon$	incremental principal plastic strain

633

634 **Table 1. Summary of soil properties for five sites in the Gulf of Mexico**

Site	Depth below mudline, z: m		Shear strength, s_u: kPa		Relative density; I_D (%)	Friction, dilation angles; ϕ', ψ (°)	Submerged unit weight, γ': kN/m^3	Soil type
	Top	Bottom	s_{um} (kPa)	k (kPa/m)				
1	0.00	2.70	-	-	22.7	33.1, 4.4	9.1	Loose sand
	2.70	6.10	10.30	-0.23	-	-	4.7	Very soft olive grey clay
	6.10	10.70	-	-	24.4	32.3, 2.8	7.9	Loose sand
	10.70	27.10	14.49	1.19	-	-	6.3	Soft to firm olive grey clay
2	0.00	7.00	-	-	64.9	40.7, 20.1	9.4	Medium grey fine sand
	7.00	56.1	17.87	1.31	-	-	6.7	Soft to stiff grey clay
3	0.00	4.90	-	-	63.7	41.1, 21.1	9.4	Medium sand
	4.90	52.10	22.13	0.93	-	-	7.3	Soft to stiff grey clay
4	0.00	4.30	-	-	86.2	46.3, 32.0	8.5	Very dense sand
	4.30	9.60	37.42	5.71	-	-	6.6	Firm to stiff dark greenish grey clay
5	0.00	3.05	-	-	43.1	37.6, 13.7	8.6	Medium sand
	3.05	12.80	27.45	1.94	-	-	7.5	Firm olive grey lean clay
			18.77*	2.65*				

635
636 * Undrained shear strength derived from the weighted average method.

637 **Table 2. Summary of jack-up rig and spudcan details**

Site	**Jack-up rig type**	**Equivalent diameter, D: m**	**Spudcan bearing area, A: m^2**	**Spudcan volume, V: m^3**	**Spudcan volume below the maximum diameter, V_b: m^3**	**Lightship + Variable load per spudcan, Q_L: MN**	**Maximum preload per spudcan, Q_P: MN**	**Maximum bearing pressure, q_{max}: kPa**
1	MLT 82-SDC	12.1	114.7	287.7	122.7	22.7	35.5	309.5
2	MLT 116-C	13.5	143.6	382.8	75.2	35.4	53.4	371.9
3	MLT 82-SDC	12.1	114.7	287.7	122.7	22.7	35.6	310.4
4	MLT 116-C	13.5	143.6	382.8	75.2	33.4	56.0	390.0
5	MLT 82-SDC	12.1	114.7	287.7	122.7	22.7	35.6	310.8

638 **Table 3. Summary of relative density equations and the derived values**

Literature	Equations	Relative density: I_D (%)				
		Site 1	Site 2	Site 3	Site 4	Site 5
Terzaghi and Peck (1967)	$I_D(\%) = 100\sqrt{(N_1)_{60} / 60}$	22.6	64.7	63.5	85.9	43.0
		24.3				
Skempton (1986)	$I_D(\%) = 100\sqrt{\frac{0.5\log\left(\frac{2000}{\sigma'_{v0}}\right)N_{60}}{55}}$	23.6	67.6	66.3	89.7	44.9
		25.4				
Kulhawy and Mayne (1990)	$I_D(\%) = 100\sqrt{\frac{(N_1)_{60}}{[60 + 25\log_{10}(D_{50})]OCR^{0.18}}}$	21.8	62.4	61.2	82.8	41.4
		23.4				
Average I_D (%)		**22.7**	**64.9**	**63.7**	**86.2**	**43.1**
		24.4				

639

640

641

642

643

644

645

646

647

648

649

Number of figure: 6

Figure 1. Spudcan geometry and dimensions: (a) Marathon LeTourneau Design Class 82-SDC (MLT 82-SDC); (b) Marathon LeTourneau Design Class 116-C (MLT 116-C)

Figure 2. Site 1: (a) Undrained shear strength profiles of two clay layers; (b) Comparison of measured, predicted and computed load-penetration profiles

Figure 3. Site 2: (a) Undrained shear strength profiles of two clay layers; (b) Comparison of measured, predicted and computed load-penetration profiles

Figure 4. Site 3: (a) Undrained shear strength profiles of two clay layers; (b) Comparison of measured, predicted and computed load-penetration profiles

Figure 5. Site 4: (a) Undrained shear strength profiles of two clay layers; (b) Comparison of measured, predicted and computed load-penetration profiles

Figure 6. Site 5: (a) Undrained shear strength profiles of two clay layers; (b) Comparison of measured, predicted and computed load-penetration profiles

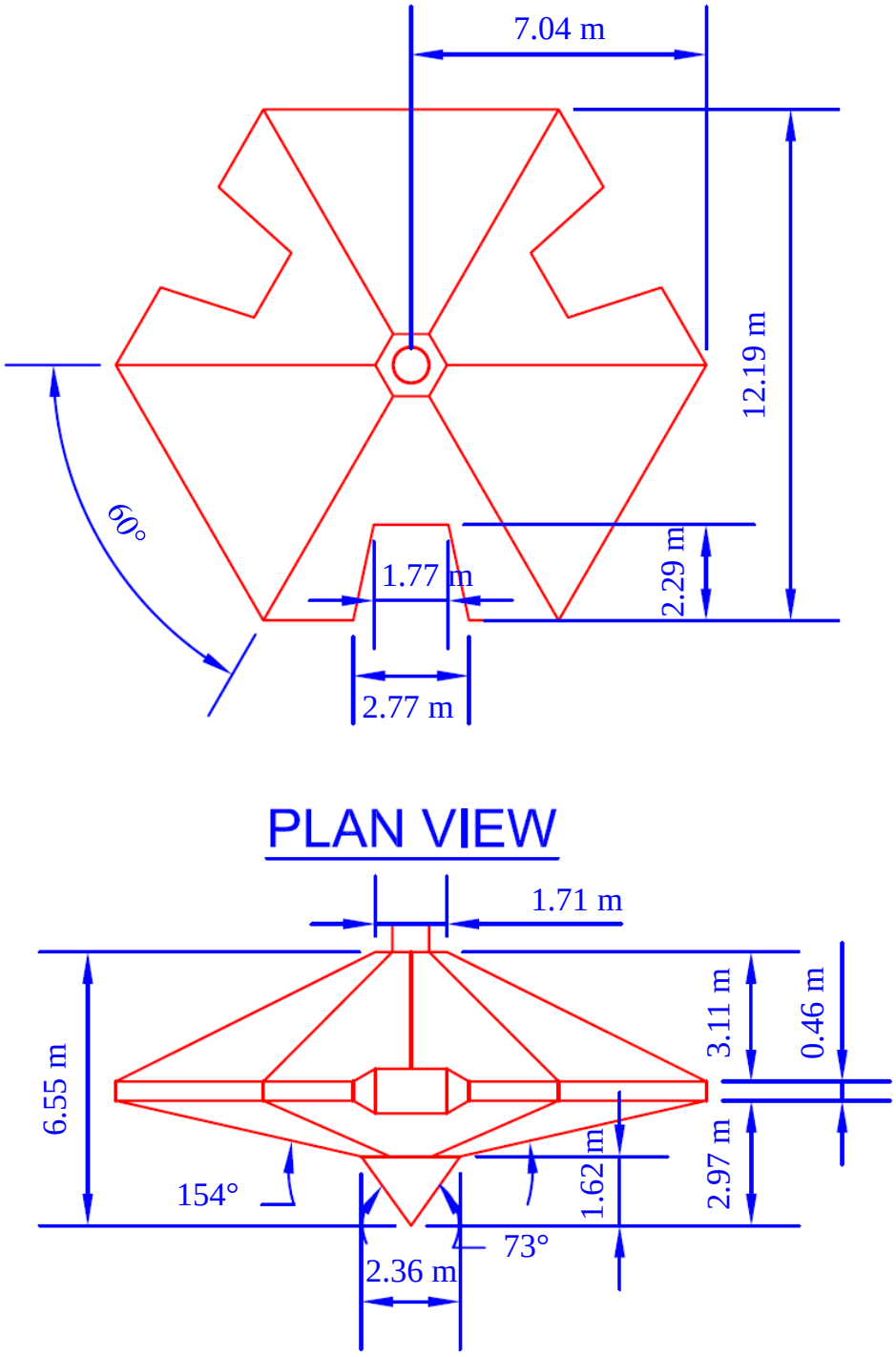

(a) Marathon LeTourneau Design Class 82-SDC (MLT 82-SDC)

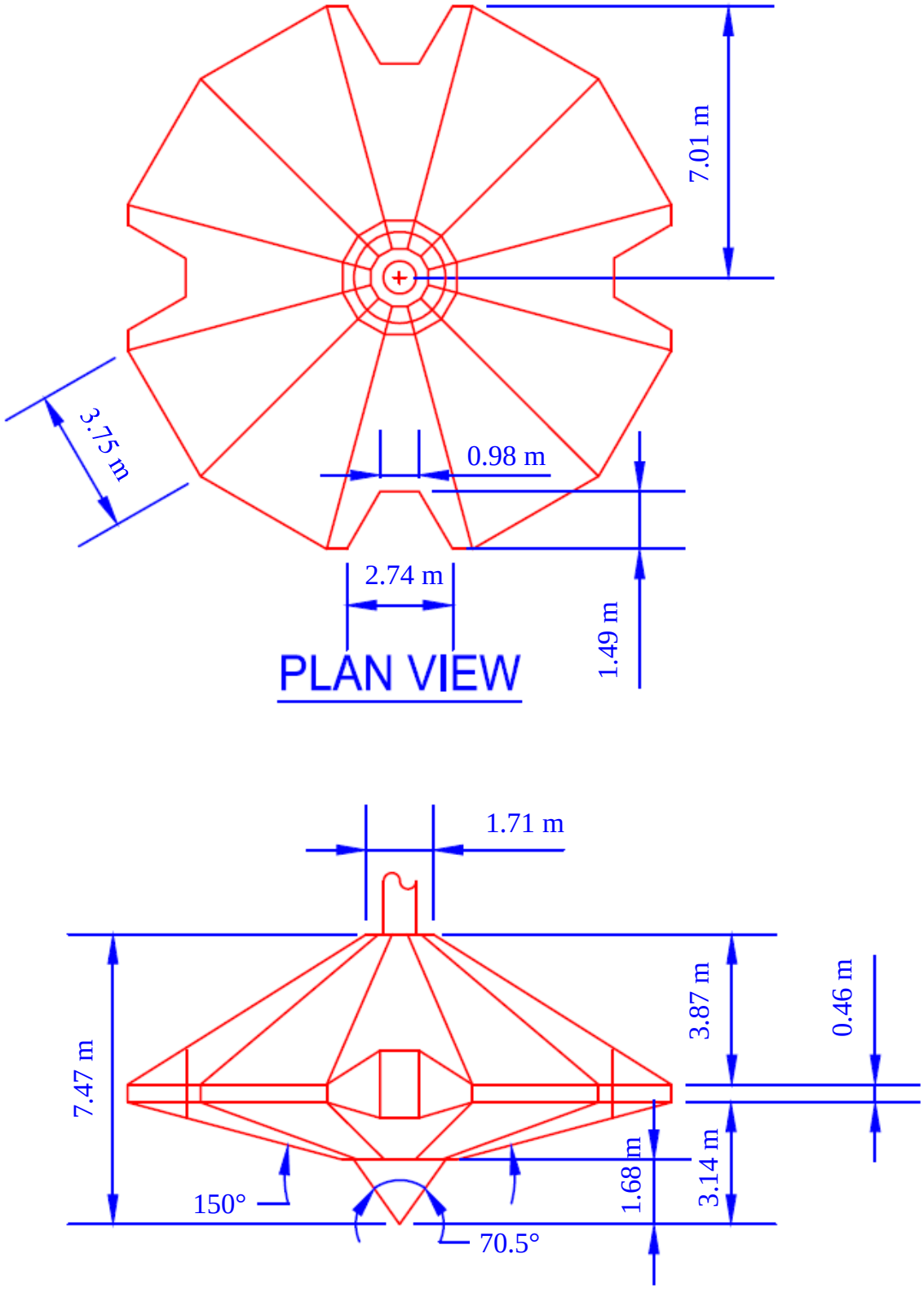

(b) Marathon LeTourneau Design Class 116-C (MLT 116-C)

Fig. 1. Spudcan geometry and dimensions

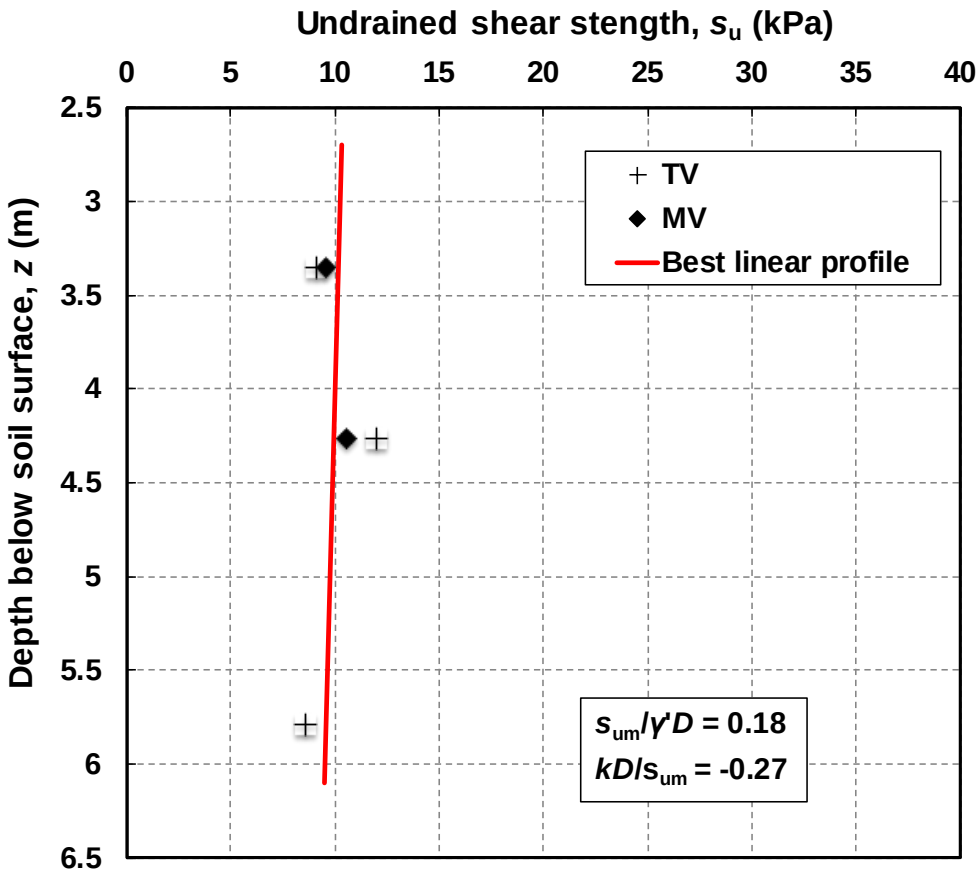
Undrained shear stength, s_u (kPa)
0
5
10
15
20
25
30
35
40
Depth below soil surface, z (m)
2.5
3
3.5
4
4.5
5
5.5
6
6.5
TV
MV
Best linear profile
$s_{um}/\gamma' D$ = 0.18
kD/s_{um} = -0.27

680
681
682

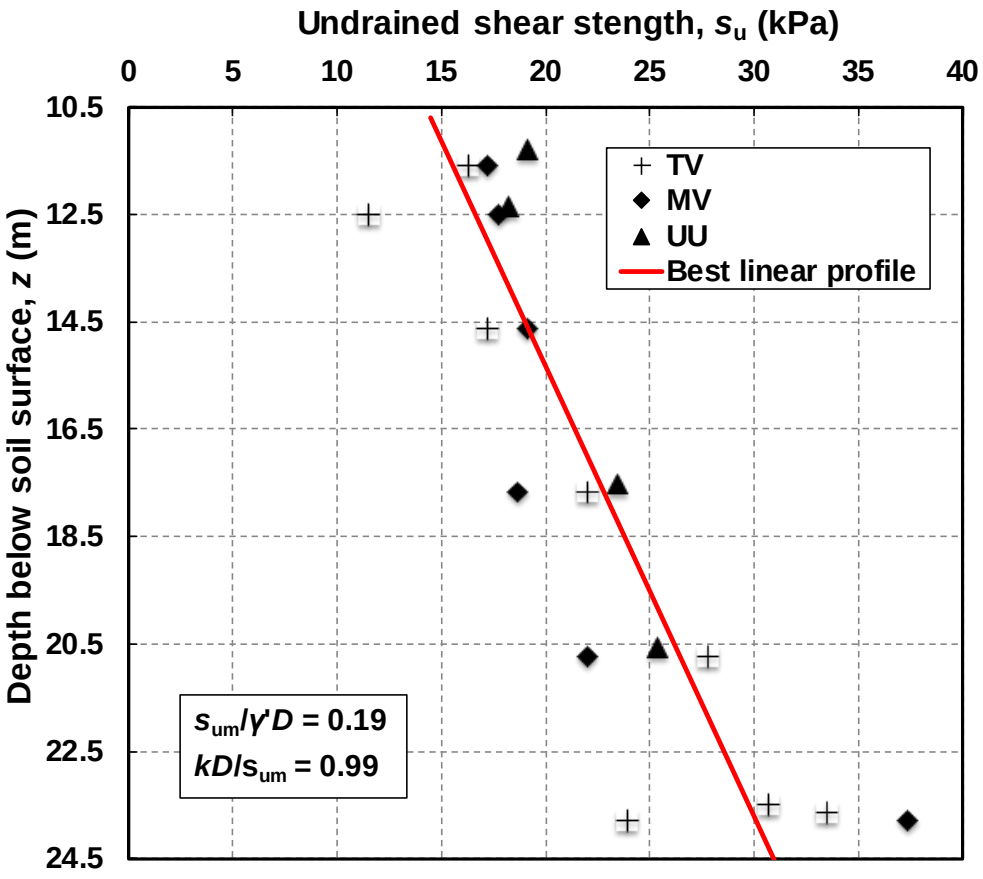

683

684 a) Undrained shear strength profiles of two clay layers

685

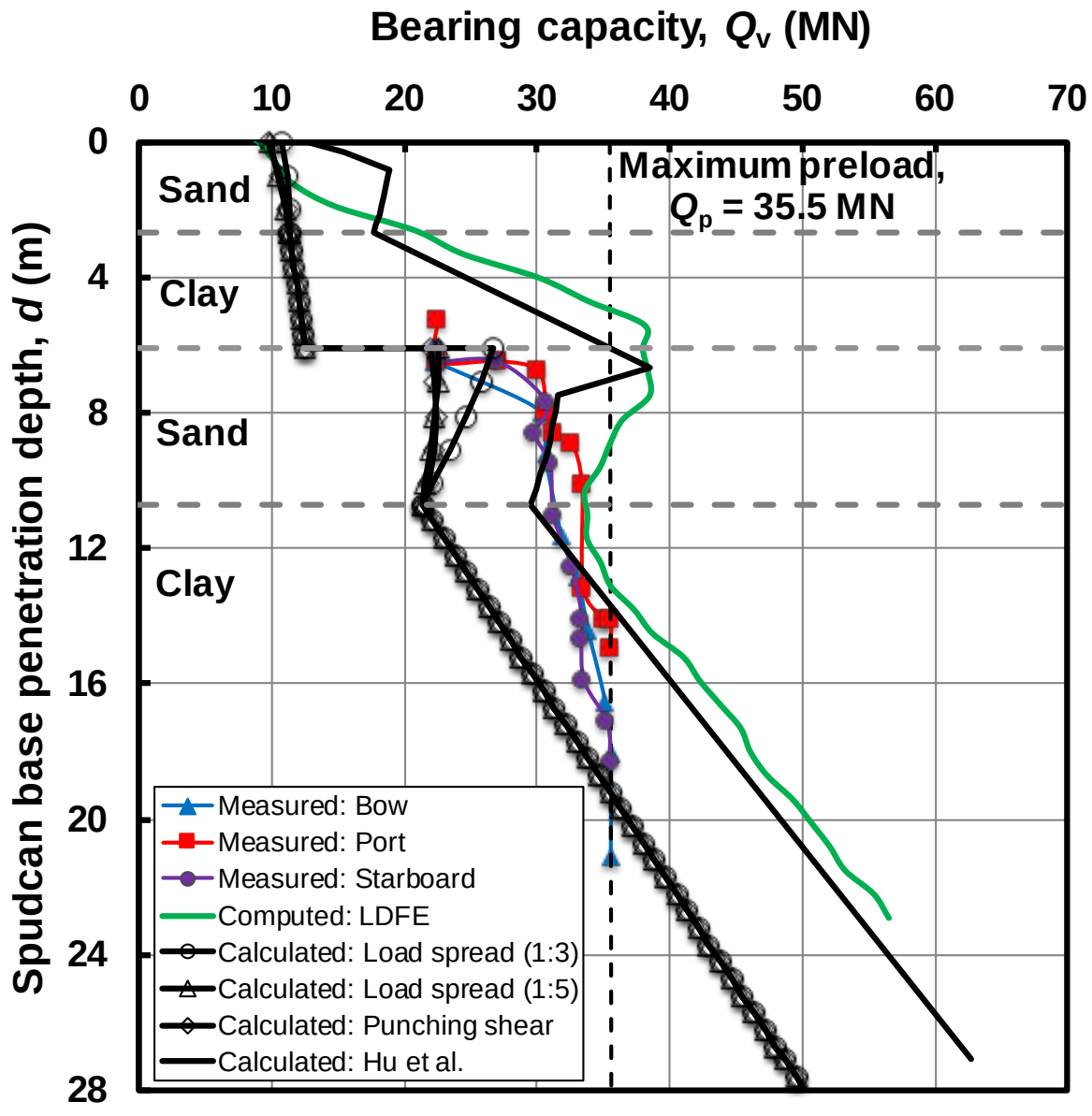

(b) Comparison of measured, predicted and computed load-penetration profiles

Fig. 2. Site 1: (a) Undrained shear strength profiles of two clay layers; (b) Comparison of measured, predicted and computed load-penetration profiles

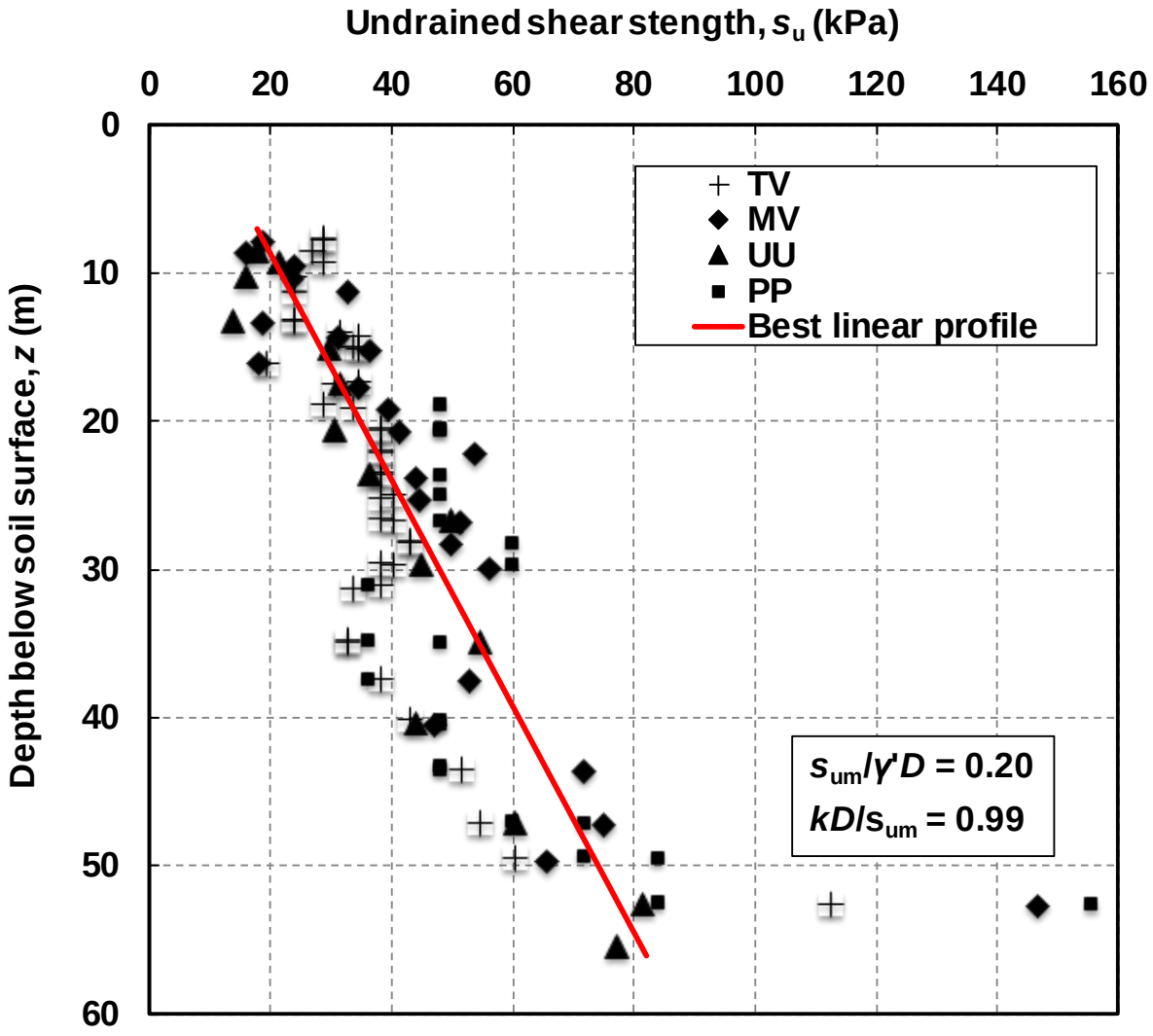

(a) Undrained shear strength profile of the clay layer

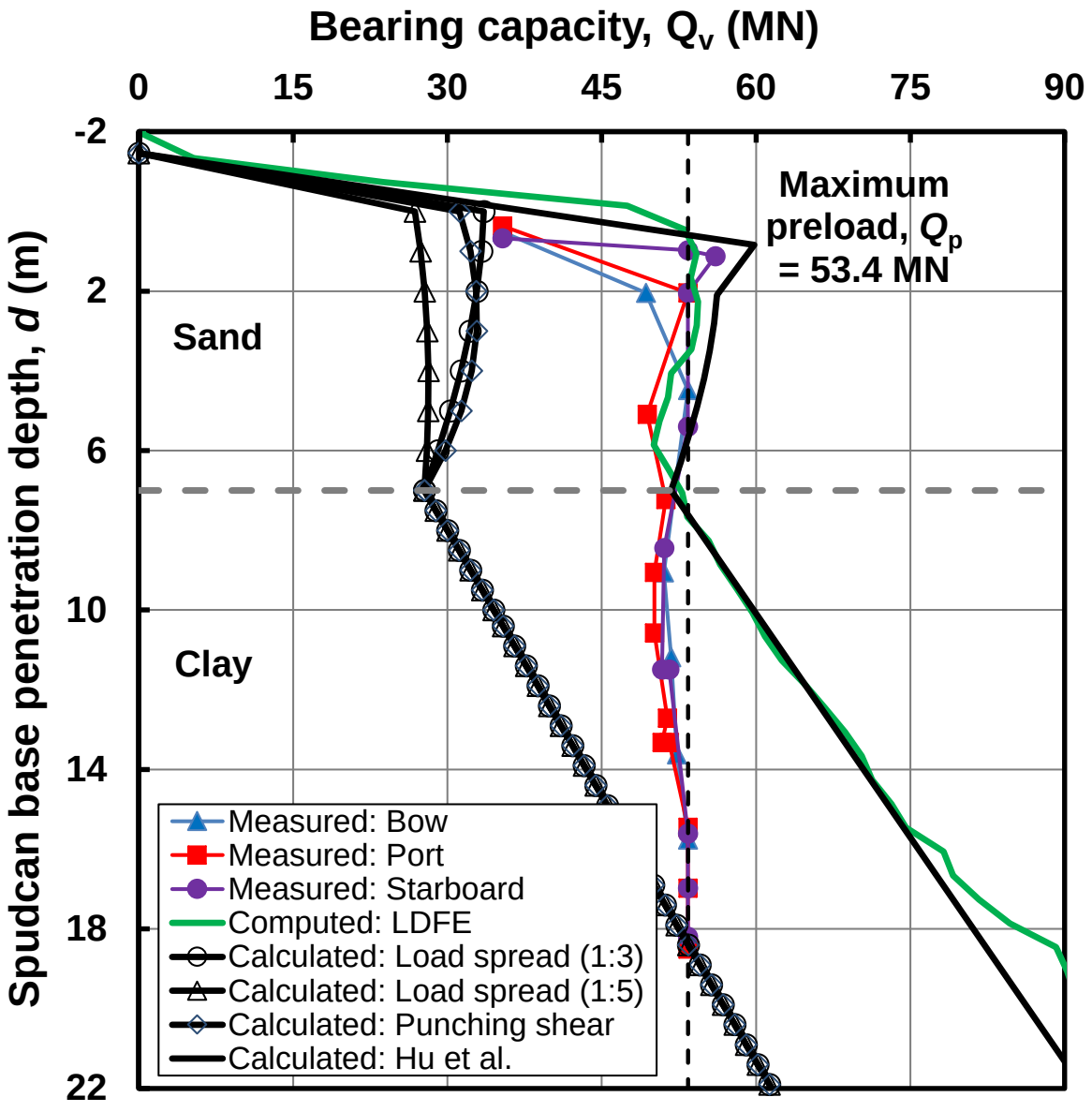

(b) Comparison of measured, predicted and computed load-penetration profiles

Fig. 3. Site 2: (a) Undrained shear strength profile of the clay layer; (b) Comparison of measured, predicted and computed load-penetration profiles

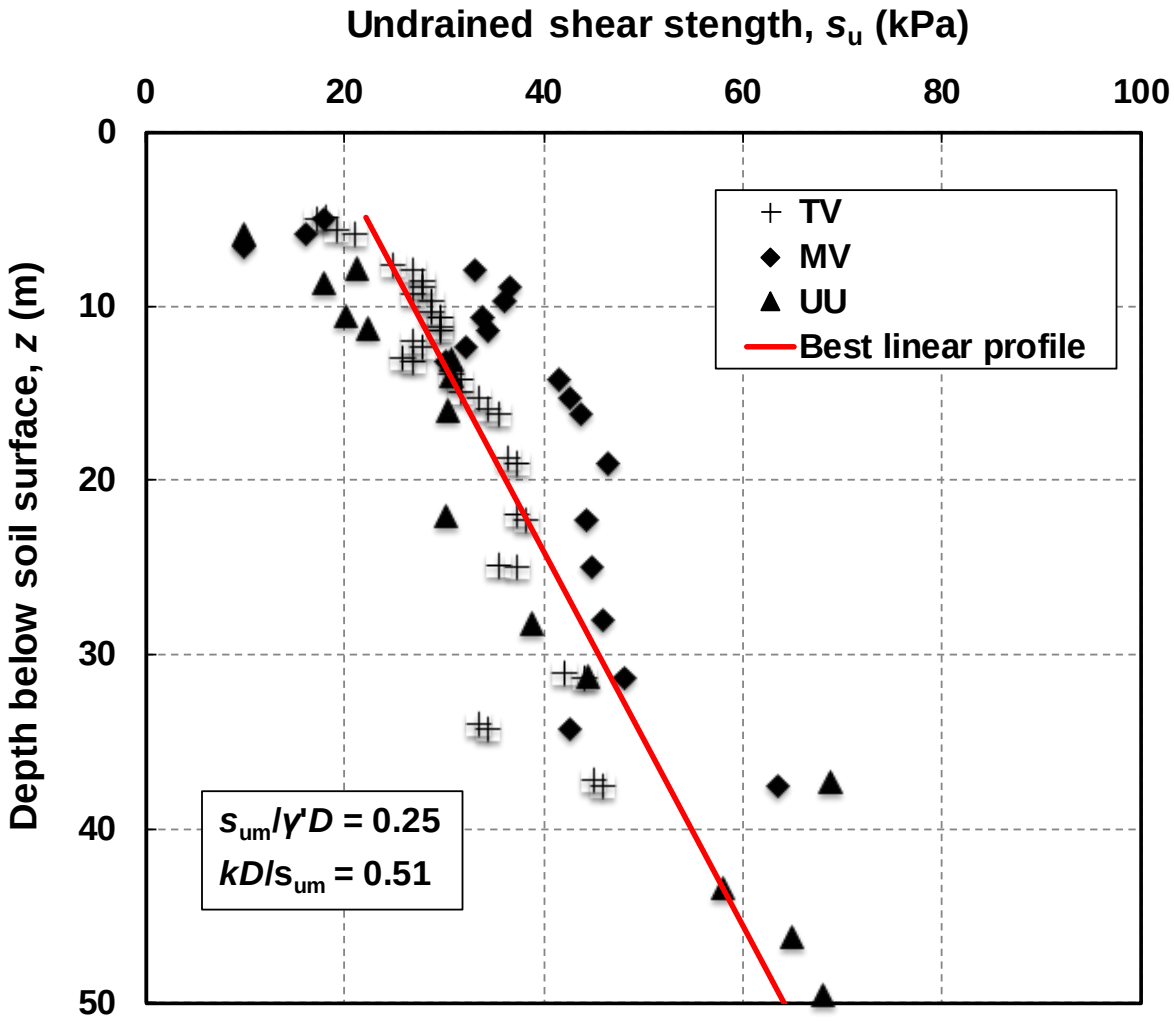

(a) Undrained shear strength profile of the clay layer

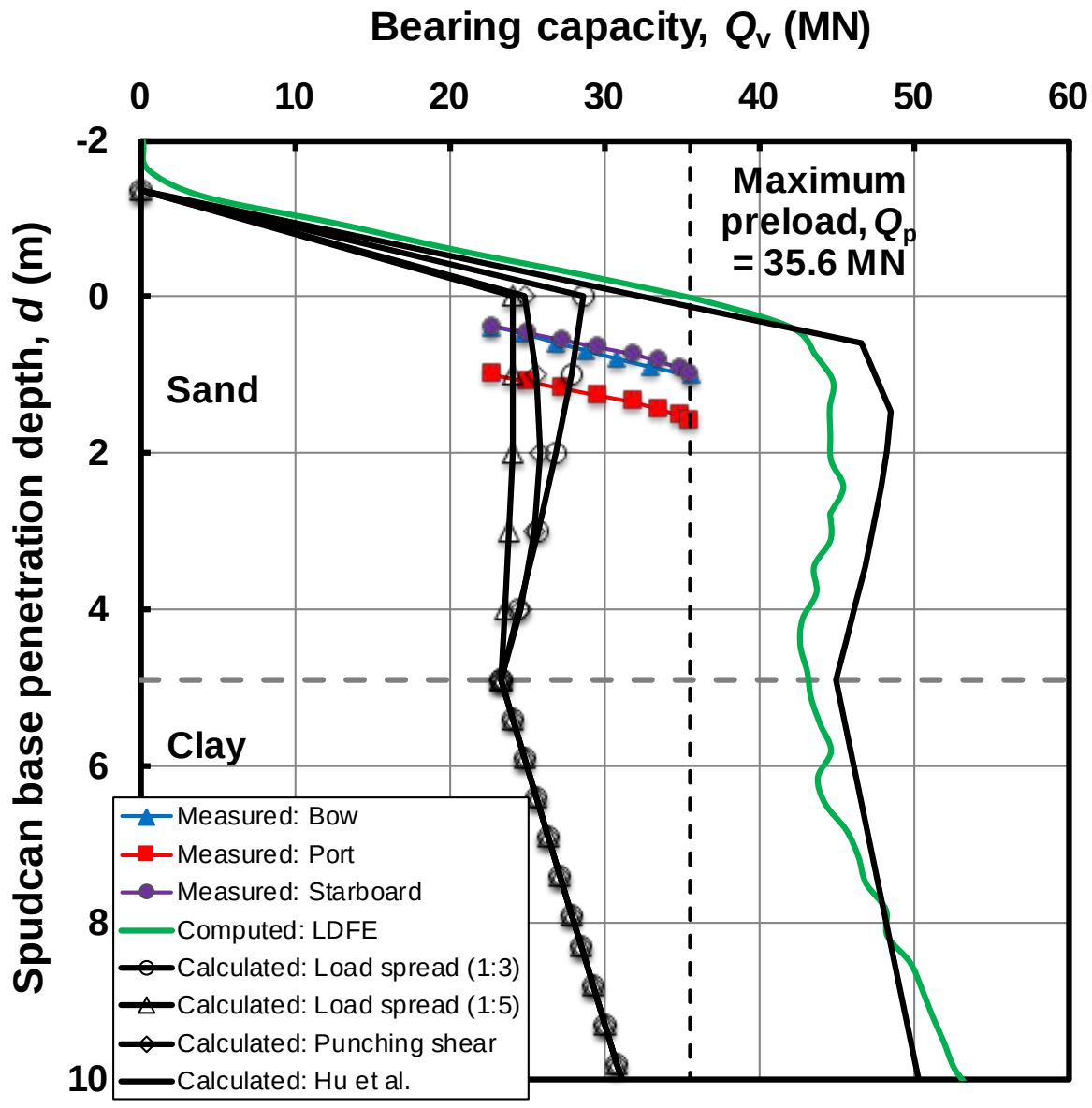

(b) Comparison of measured, predicted and computed load-penetration profiles

Fig. 4. Site 3: (a) Undrained shear strength profile of the clay layer; (b) Comparison of measured, predicted and computed load-penetration profiles

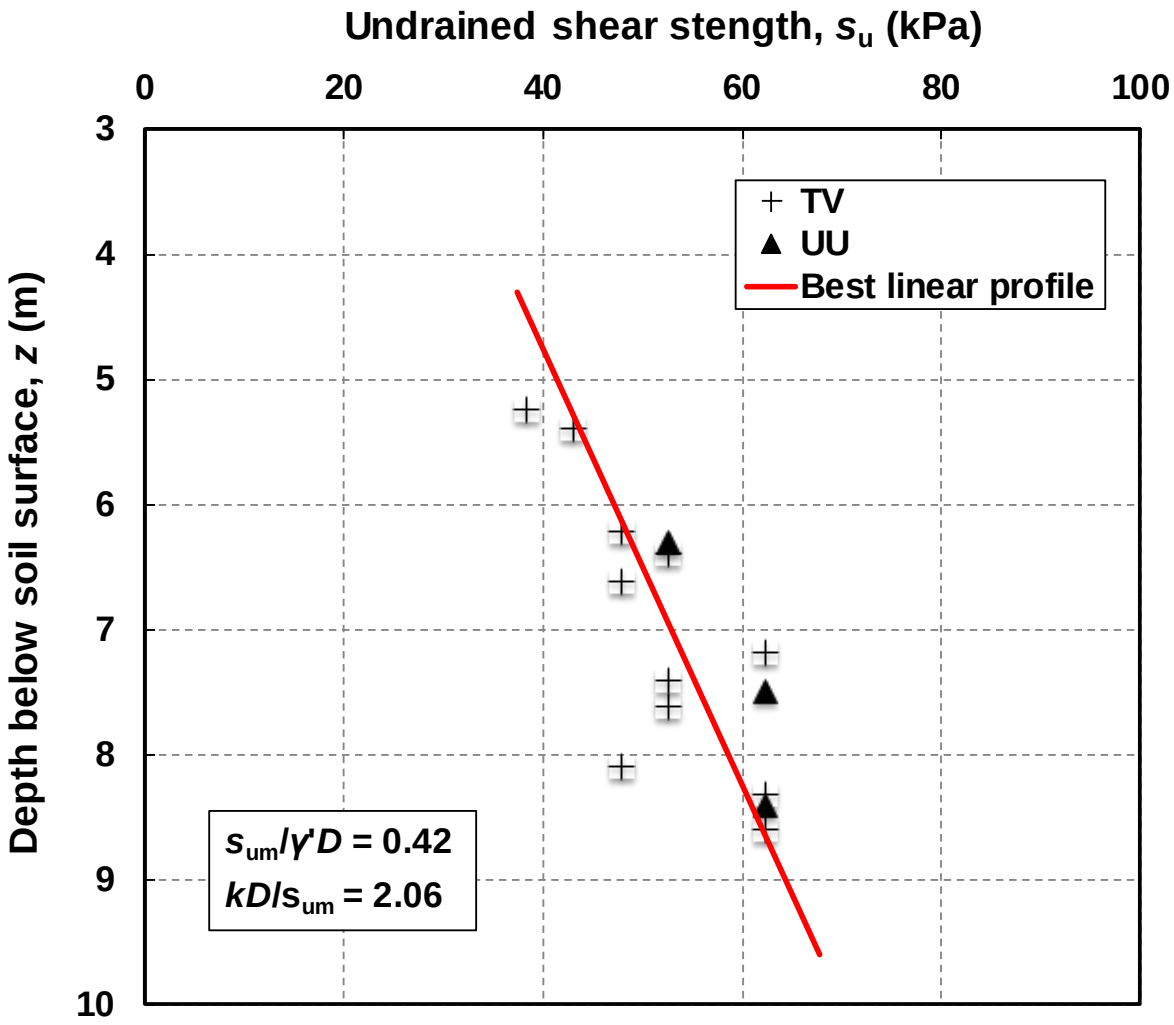

(a) Undrained shear strength profile of the clay layer

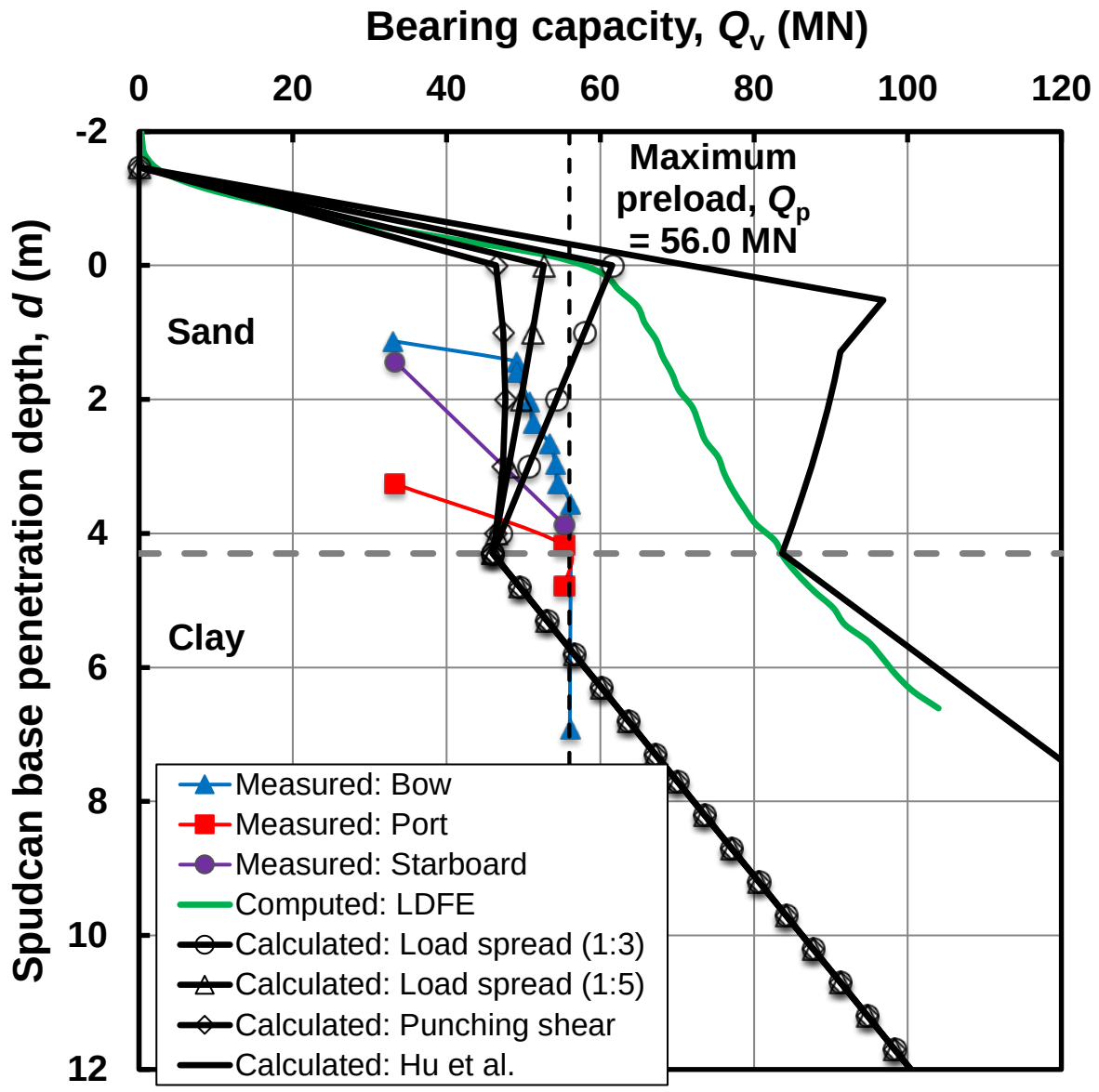

(b) Comparison of measured, predicted and computed load-penetration profiles

Fig. 5. Site 4: (a) Undrained shear strength profile of the clay layer; (b) Comparison of measured, predicted and computed load-penetration profiles

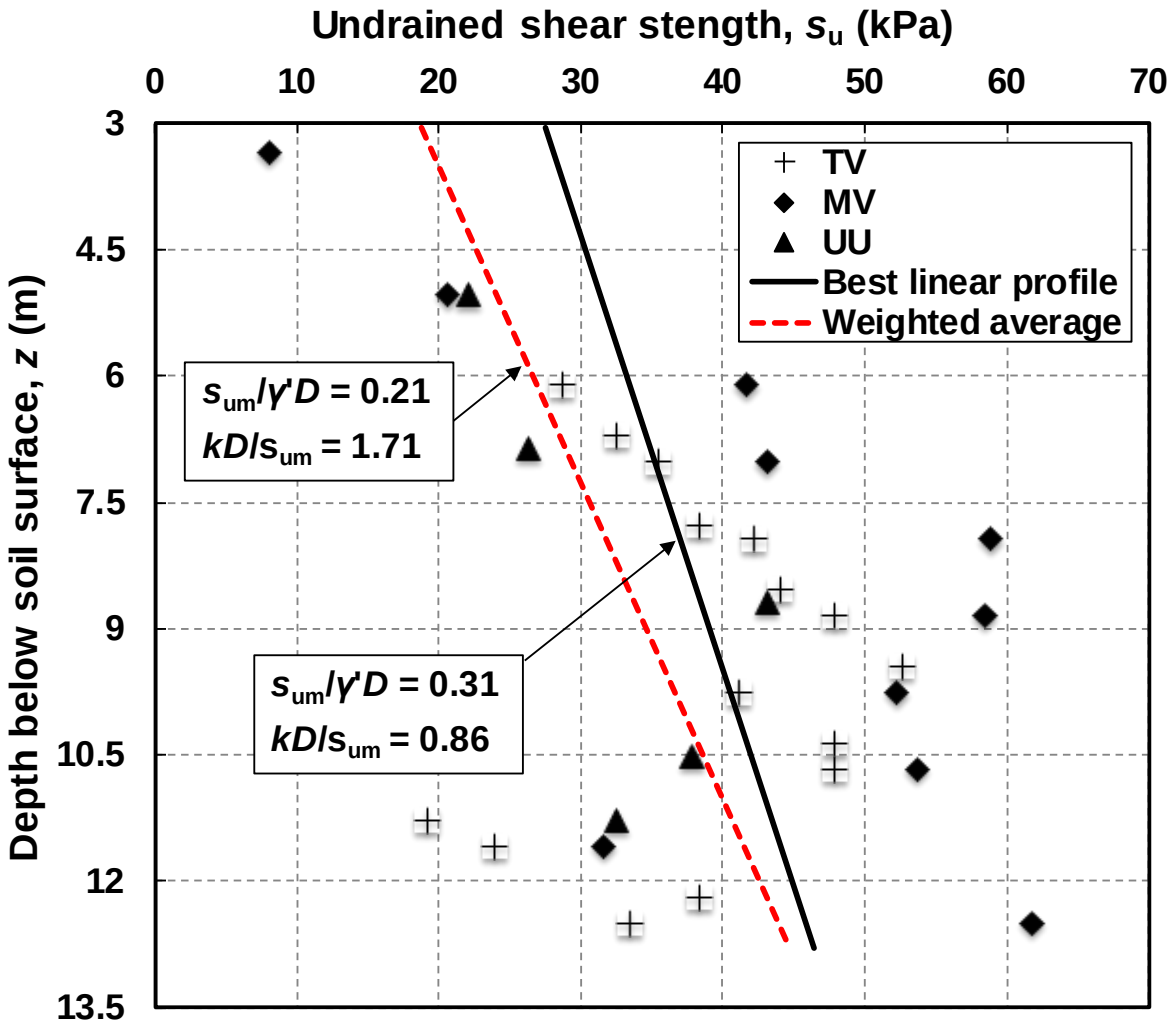

(a) Undrained shear strength profile of the clay layer

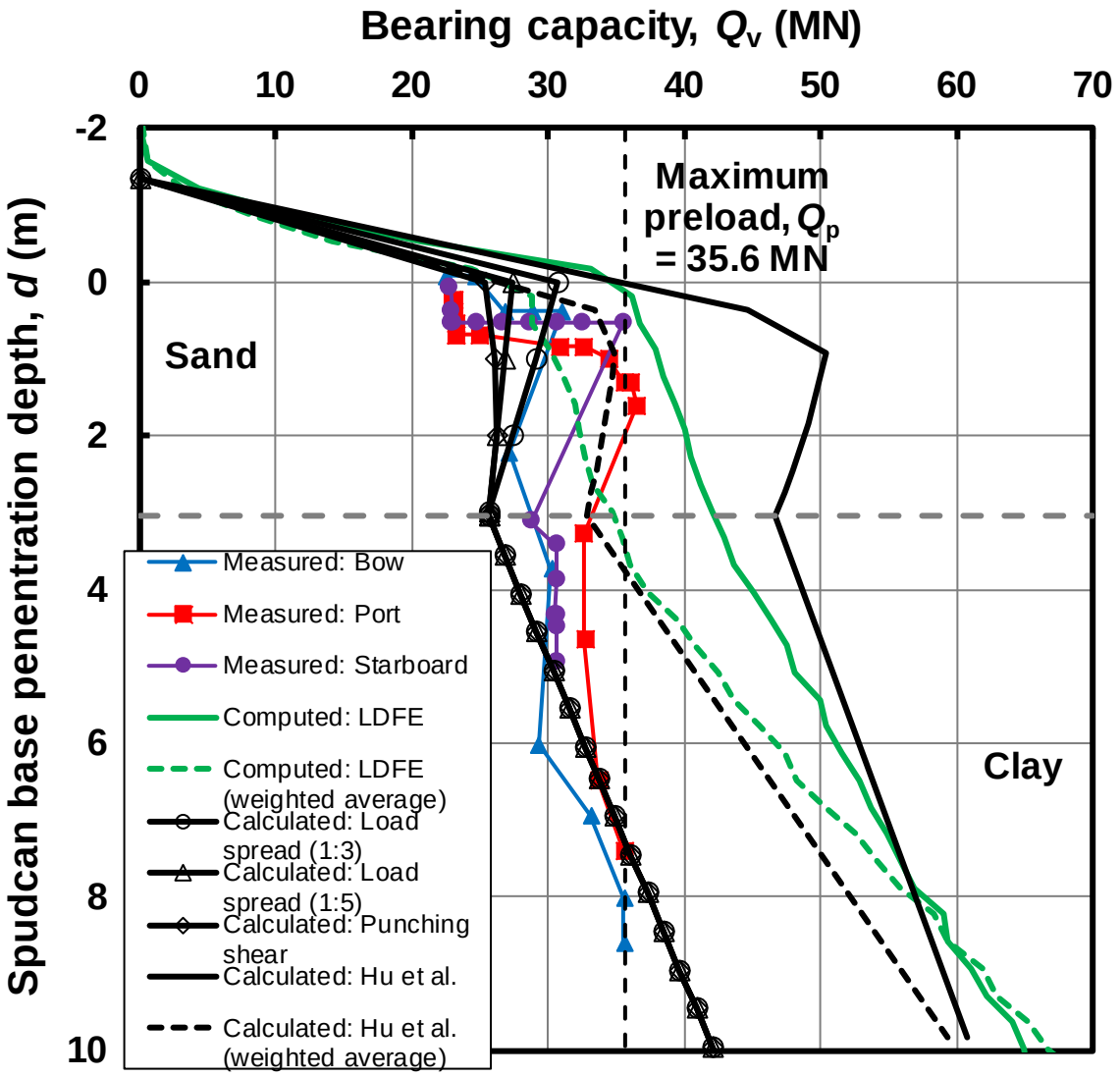

(b) Comparison of measured, predicted and computed load-penetration profiles

Fig. 6. Site 5: (a) Undrained shear strength profile of the clay layer; (b) Comparison of measured, predicted and computed load-penetration profiles

APPENDIX

Table 1. Full profile design equations for the ISO methods and Hu et al. approach

Method	Equations	Input variables	
ISO methods	Load spread method: $Q_v = Q_{u,b} - 0.25\pi\left(D + 2\frac{t}{n_s}\right)^2 t\gamma'_s$ (1) $Q_{u,b} = s_u N_c 0.25\pi\left(D + 2\frac{t}{n_s}\right)^2 + \gamma'_s\left[0.25\pi\left(D + 2\frac{t}{n_s}\right)^2 H_s + V_b\right]$ (2) Punching shear method: $Q_v = Q_{u,b} - 0.25\pi D^2 t\gamma'_s + 0.5\pi D^2 t\left[t\gamma'_s + 2\gamma'_s\left(H_s - t\right)\right]\frac{K_s \tan\phi'}{D}$ (3) $Q_{u,b} = s_u N_c\left(0.25\pi D^2\right) + \gamma'_s\left(0.25\pi D^2 H_s + V_b\right)$ (4)	d D D_F E E^* H_{plug} H_s k K_s n_s N_c N_{c0}	penetration depth of spudcan base diameter of the spudcan distribution factor parameter to simplify the algebra parameter to simplify the algebra sand plug height sand thickness strength gradient of clay punching shear coefficient load spread factor bearing capacity factor bearing capacity factor of clay at base level of a circular foundation
Hu et al. approach	$q_{peak} = \left(N_{c0}s_{um} + q_0 + 0.12\gamma'_s H_s\right)\left(1 + \frac{1.76H_s}{D}\tan\psi\right)^{E^*}$ $+ \frac{\gamma'_s D}{2\tan\psi(E^*+1)}\left[1 - \left(1 - \frac{1.76H_s}{D}E^*\tan\psi\right)\left(1 + \frac{1.76H_s}{D}\tan\psi\right)^{E^*}\right]$ (5) $N_{c0} = 6.34 + 0.56\frac{k\left(D + 1.76H_s\tan\psi\right)}{s_{um}}$ (6) $E^* = 2\left[1 + D_F\left(\frac{\tan\phi^*}{\tan\psi} - 1\right)\right]$ (7) $D_F = 0.642\left(\frac{H_s}{D}\right)^{-0.576}$ *as* $0.16 \le \frac{H_s}{D} \le 1.0$ (8)	q_0 q_{clay} $Q_{u,b}$ Q_v s_u s_{u0} s_{um} t V_b γ'_c γ'_s ϕ' ϕ^*	effective overburden pressure penetration resistance in the clay layer ultimate vertical bearing capacity of the fictitious footing vertical bearing capacity of a spudcan undrained shear strength of clay clay shear strength at lowest level of the spudcan widest cross-sectional area shear strength of clay at sand-clay interface thickness of the sand layer in the ISO methods volume of spudcan below maximum bearing area effective unit weight of clay effective unit weight of sand friction angle of sand reduced friction angle due to non-associated flow rule

	$D_F = 0.623\left(\frac{H_s}{D}\right)^{-0.174}$ *as* $0.21 \le \frac{H_s}{D} \le 1.12$ (9) $\tan\phi^* = \frac{\sin\phi'\cos\psi}{1-\sin\phi'\sin\psi}$ (10) $q = \frac{\gamma'_S D}{E} + \left\{\begin{array}{l}\left[\left(14.8\frac{d-0.1H_S}{D}+10.6\right)s_u + q_0 + \gamma'_S H_S + \right.\\ \left.\left(\gamma'_C-\gamma'_S\right)\left(d-0.1H_S\right)-\frac{\gamma'_S D}{E}\right]\\ \exp\left[\frac{E\left(H_S-d\right)}{D}\right]\end{array}\right\}$ (11) $E = 4D_F\sin\phi_{cv}$ (12) $D_F = 0.50\left(\frac{H_s}{D}\right)^{-0.389}$ for $0.3H_s \le d < H_s$ (13) $D_F = 0.40\left(\frac{H_s}{D}\right)^{-0.063}$ for $0.3H_s \le d < H_s$ (14) $q_{clay} = N_c s_{u0} + H_{plug}\gamma'_c = N_c s_{u0} + 0.9H_s\gamma'_c \quad \left(0.16 \le \frac{H_s}{D} \le 1.00\right)$ (15) $N_c = \left(9 + 0.9\frac{kD}{s_{um}}\right) + \left(10 + \frac{kD}{s_{um}}\right)\frac{H_s}{D} \quad \left(\text{for} \quad 0 \le \frac{kD}{s_{um}} \le 3\right)$ (16)	ψ	dilation angle of sand